

Absolute photodissociation cross sections of gas phase sodium chloride at room temperature

J. A. Silver, D. R. Worsnop, A. Freedman, and C. E. Kolb

Citation: *The Journal of Chemical Physics* **84**, 4378 (1986); doi: 10.1063/1.450060

View online: <http://dx.doi.org/10.1063/1.450060>

View Table of Contents: <http://scitation.aip.org/content/aip/journal/jcp/84/8?ver=pdfcov>

Published by the [AIP Publishing](#)

Articles you may be interested in

[Absolute cross sections of ozone at atmospheric temperatures for the Wulf and the Chappuis bands](#)

J. Chem. Phys. **122**, 244311 (2005); 10.1063/1.1937369

[The absolute cross sections of photoabsorption, photodissociation, and photoionization of the group VIB metal hexacarbonyls at 300–1600 Å](#)

J. Chem. Phys. **106**, 9474 (1997); 10.1063/1.474077

[Absolute absorption cross sections of gas phase C₆₀ at 600°C](#)

J. Chem. Phys. **97**, 3855 (1992); 10.1063/1.462967

[Absolute Specific Photodissociation Cross Sections of CH₄ in the Extreme Ultraviolet](#)

J. Chem. Phys. **57**, 286 (1972); 10.1063/1.1677958

[Measurements of Absolute Total Cross Sections for Rare Gas Scattering](#)

J. Chem. Phys. **43**, 4177 (1965); 10.1063/1.1696664



Absolute photodissociation cross sections of gas phase sodium chloride at room temperature

J. A. Silver,^{a)} D. R. Worsnop, A. Freedman, and C. E. Kolb

Center for Chemical and Environmental Physics, Aerodyne Research, Inc., Billerica, Massachusetts 01821

(Received 12 December 1985; accepted 2 January 1986)

Absolute photodissociation cross sections for gas phase NaCl are measured over the wavelength range of 189.7–359.8 nm at 300 K. Two well-resolved peaks are observed at 235 and 260 nm. The cross section also rises below 210 nm. These results are in good qualitative agreement with previous high temperature measurements and with cross sections computed from theoretically calculated potential surfaces. However, there are two significant differences, the spectral width and the absolute magnitude of the cross sections. The importance of these measurements in understanding the photodissociative processes of ionic compounds and the implications for the role of NaCl in the stratospheric chemistry of chlorine compounds are discussed.

INTRODUCTION

The study of the optical spectra of gas phase alkali halides has a long and rich history,¹ having been pursued in flames,^{2,3} furnaces,⁴ shock tubes,⁵ and more recently, in room temperature cells⁶ and molecular beams.^{3,7–11} In conjunction with these experimental studies, the theory of photodissociation of alkali halides has received considerable attention.^{1,12–14} Photodissociative processes for these systems are often approximated as one-electron charge transfers between a ground ionic state and excited covalent state. Measurement of the spectrally resolved cross sections and determination of the relative probability of exciting parallel ($0^+ \leftarrow \Sigma^+$) and perpendicular ($1 \leftarrow ^1\Sigma^+$) transitions lead to information about the shapes of the excited state potentials. Combined with product analysis, one can then learn how dissociation from the 0^+ excited states is affected by the degree of adiabatic behavior in the exit channel when crossing the ionic $^1\Sigma^+$ potential curve.

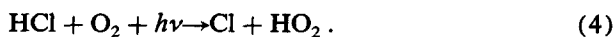
The measurement of photodissociation cross section is also of interest in understanding the chemistry of alkali metals in the stratosphere. It has been suggested^{15–17} that sodium and other metals introduced into the atmosphere by meteor or ablation may play a role in affecting ozone reduction by the catalytic chlorine cycle. One possible reaction sequence which demonstrates this mechanism is



and



which leads to the net reaction



Rate constants for reactions (1) and (2) have been measured in our laboratory.^{18,19} Combining these results with photolysis rates based on the high temperature absorption measurements (1123–1223 K) of Davidovits and Brodhead,^{4,17} leads to the possibility that this mechanism could

be comparable in magnitude to the major stratospheric Cl regeneration mechanism,



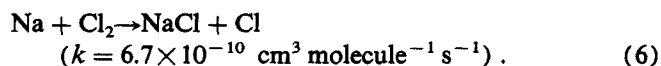
The rate limiting step of the sodium catalyzed mechanism [reactions (1)–(3)] is reaction (3). Davidovits' absorption data include contributions from vibrationally excited states and possibly dimers, which will not contribute to photolysis at stratospheric temperatures near 260 K. Clearly, low temperature photodissociation cross section measurements are desirable.

In this paper we report measurements of the absolute cross section for photodissociation of NaCl at 300 K. Sodium chloride is produced by the gas phase reaction of atomic sodium with chlorine in a flow tube under dimer-free conditions and with over 80% of the NaCl in the ground vibrational state. The approach taken in these experiments does not require the knowledge of the absolute NaCl number density in the photolysis region, but rather uses a ratio technique to quantify the cross sections.

EXPERIMENTAL

Photodissociation apparatus

Sodium chloride is generated in a flow tube by the fast bimolecular reaction of atomic sodium with excess chlorine,²⁰



Sodium atoms are generated by heating sodium metal in a 2 cm diam cylindrical stainless steel oven to ~ 510 K which produces a vapor pressure of $\sim 2 \times 10^{-3}$ Torr within the oven. The vapor is entrained in a flow of helium, and carried through a heated 0.6 cm diam 40 cm long stainless steel tube into the flow apparatus. This heated tube is wrapped with ~ 0.3 cm thick zirconia blanket insulation and enclosed in a water cooled jacket to prevent any heating of the main flow carrier gas. The sodium vapor is diluted by the carrier gas in the main flow so that the sodium or sodium chloride concentration within the photolysis zone is always less than 10^{10} cm^{-3} . Chlorine is mixed with the main carrier flow and its reaction with sodium is complete within a few centimeters of the sodium inlet orifice.

^{a)} Present address: Southwest Sciences, Inc., 1570 Pacheco St., Suite E-11, Santa Fe, NM 87501.

OPTICAL LAYOUT FOR MEASUREMENT OF PHOTODISSOCIATION CROSS SECTIONS

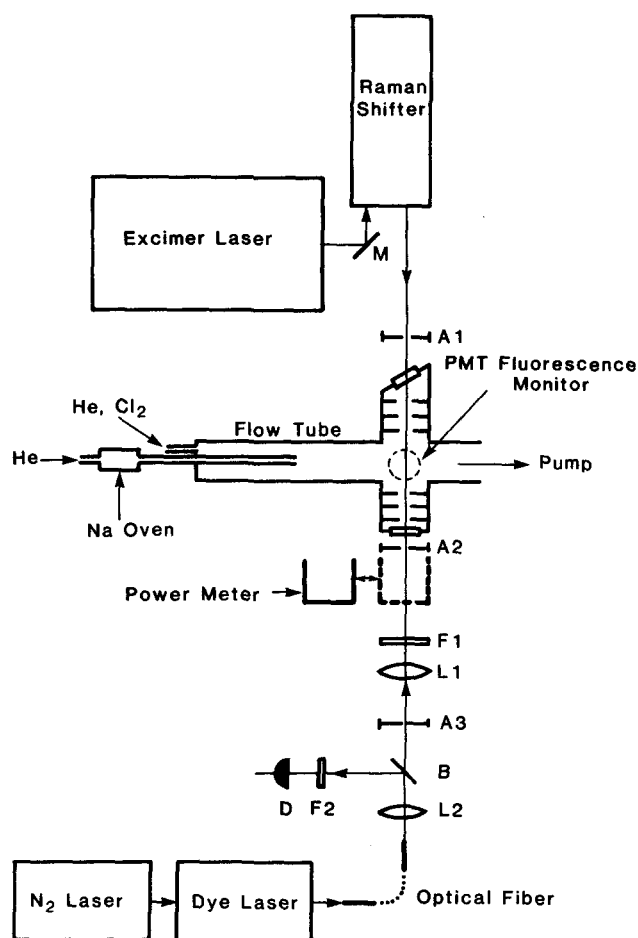


FIG. 1. Schematic of the experimental apparatus for photodissociation of NaCl. Components are identified as follows: M = mirror; A1, A2, and A3 = apertures; F1 = BK-7 window acting as a UV absorbing filter; F2 = 590 nm interference filter; L1 and L2 = lenses; B = quartz slide acting as a beamsplitter; D = fast UV photodiode detector.

The flow apparatus is comprised of a small stainless steel tube 9.7 cm in diameter and approximately 50 cm long, with four perpendicular side arms at the detection zone which permit photodissociation and detection of the flow species (Fig. 1). The main flow of helium carrier gas is added at the entrance of the flow tube and a small purge flow of helium is introduced in each of the side arms to keep the optics clean. Gas volumetric flow rates are determined with calibrated thermal conductivity-type mass flow meters. Flow rates of chlorine are determined by diverting the flow into a calibrated volume and measuring the rate of pressure increase. A calibrated MKS Baratron capacitance manometer is used to measure pressure and a chromel–alumel thermocouple is used to determine the gas temperature. Experiments are performed with a flow velocity of 150 cm s^{-1} at a pressure of 2.1 Torr.

Relative concentrations of atomic sodium are measured using laser-induced fluorescence of the $3s^2S_{1/2} - 3s^2P_{3/2}$ transition at 589.9 nm. The output of a nitrogen-pumped dye laser (Molelectron DL14) is transmitted to the experiment by

a fiber optic line and is focused in the photolysis region to a diameter of $0.380 \pm 0.005 \text{ cm}$. Fluorescence is detected by a photomultiplier located perpendicular to the laser path as shown in Fig. 1. A 590 nm interference filter and optical baffles are used to reject spurious light from entering the PMT. A 1 cm diam area of the photolysis region is imaged onto the phototube. The data are collected using a fast preamplifier and a gated integrator having a 60 ns acquisition gate width. The relative laser power in each pulse is monitored by a fast photodiode and is integrated and held until both the laser power and fluorescence signals are read into an IBM PC/XT computer for analysis.

Sodium chloride is photodissociated with a Raman-shifted excimer laser. The excimer laser (Questek) is equipped with unstable resonator optics and produces a beam with very low divergence. It uses either ArF or KrF with output pulse energies of 100–250 mJ. Its output is reflected by a dielectric-coated mirror into a Quanta Ray RS-1 Raman shifter. Using D₂, H₂, or a mixture of the two, both Stokes and anti-Stokes shifted wavelengths of the pump line are produced with pulse energies in the range 0.0023–4.4 mJ. This UV beam is focused into the cell coaxial to the dye laser beam, with care taken to ensure that the UV beam diameter is equal to or slightly less than that of the dye laser. A BK-7 window (F1 in Fig. 1) on the UV output side of the cell (visible input side) is used to absorb the UV light so that it cannot be refocused into the fiber optic or interfere with the visible power measurements. A calibrated Scientech power meter is used to monitor the average UV power as it exits the photolysis cell. Corrections are made for transmittance of the output window and spectral response of the power monitor.

Triggering of both lasers and the time delay between them (variable from 0–10 ms in 10 ns increments) is controlled by a delay generator. The excimer is triggered at a frequency (30 Hz) twice that of the dye laser, so that any nonphotodissociation related components of the signal are subtracted from the fluorescence of photodissociated sodium. The data acquisition system performs both these subtractions of background signals as well as normalization of the fluorescence to the power of each visible laser pulse. It then averages the corrected signals over a minimum of 100 pulses.

The purities of chemicals used in these experiments are as follows: sodium metal, 99.9% (Alfa); helium, 99.995% (Northeast Cryogenics); and chlorine, 99.5% (Northeast Cryogenics).

Experimental procedure and data analysis

Photodissociation cross sections are measured using a probe–pump–probe approach. The first step consists of measuring the atomic sodium concentration with no chlorine present, $[\text{Na}]_0$, in the photolysis region using the visible dye laser. Excess molecular chlorine is then added at the upstream end of the flow tube, quantitatively converting all of the Na to NaCl in a distance much shorter than the 17 cm path between the sodium oven outlet and the photolysis region. The NaCl is then photodissociated with the UV laser and the product sodium ($[\text{Na}]_p$) detected with the visible

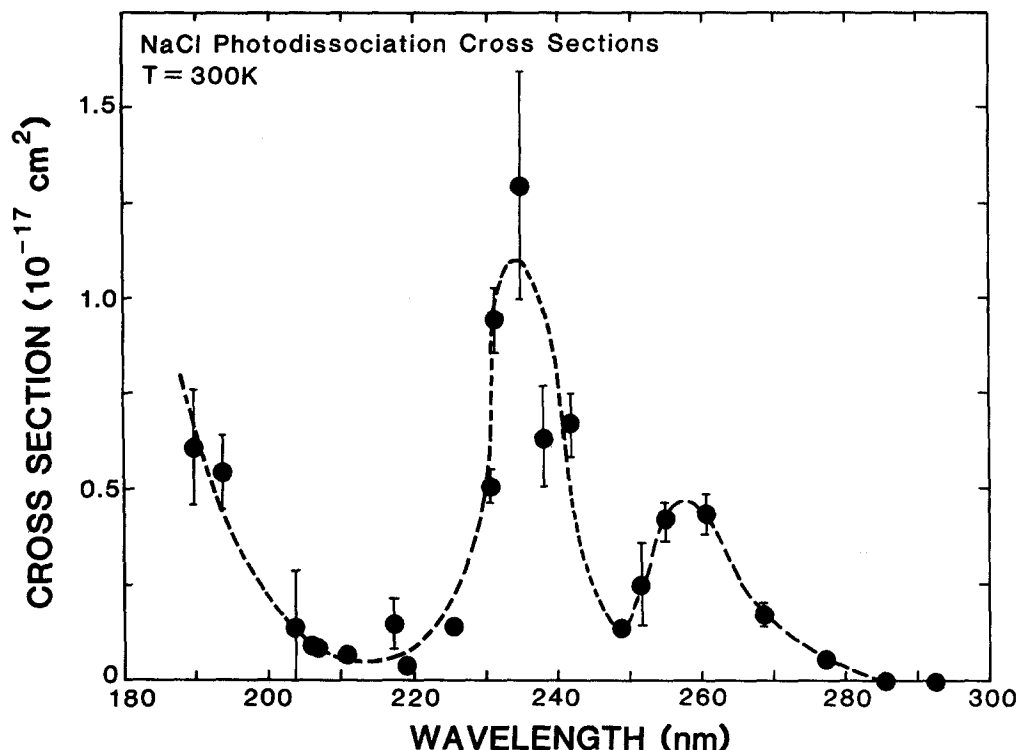


FIG. 2. Plot of experimental data vs wavelength of photodissociation cross sections for NaCl at 300 K. Error bars represent one standard deviation. A dashed curve is drawn through the points to highlight the shape of the data.

laser approximately 200 ns later. This signal is related to the initial concentration of NaCl by

$$\frac{[\text{Na}]_p}{[\text{NaCl}]} = 1 - \exp[-I(\lambda)\sigma(\lambda)], \quad (7)$$

where $I(\lambda)$ is the ultraviolet laser photon fluence per pulse at wavelength λ , and $\sigma(\lambda)$ is the photodissociation cross section at this wavelength. Because $[\text{NaCl}] = [\text{Na}]_0$, we rewrite Eq. (7),

$$R = \frac{[\text{Na}]_p}{[\text{Na}]_0} = 1 - \exp[-I(\lambda)\sigma(\lambda)]. \quad (8)$$

Since the detection techniques for measuring atomic sodium before and after the photolysis are identical, the ratio of their absolute concentrations in Eq. (8), defined as R , is equivalent to the ratio of their observed fluorescence signals. As a result, only $I(\lambda)$ need be measured absolutely.

This determination of $\sigma(\lambda)$ requires a few assumptions and clarifications. Since R depends exponentially on the UV photon flux, nonuniformities could introduce errors when using the spatially averaged value of $I(\lambda)$. This is avoided by keeping the UV beam intensity low enough so that R is always less than 0.05. Accordingly, the exponential term can be expanded and rewritten as

$$\sigma(\lambda) = \frac{R}{I(\lambda)}. \quad (9)$$

In this situation, R is linearly proportional to $I(\lambda)$, and the spatially averaged value of R is independent of any intensity nonuniformities. We confirmed the linearity of the cross section by measuring R as a function of laser intensity for some of the more intense UV lines. A linear dependence of R on $I(\lambda)$ was observed at lower intensities, becoming nonlinear at the highest intensities. We always operated in the linear regime. The intensity profile of the visible laser beam is kept

uniform to avoid nonlinearities in R .

The time delay between lasers is also critical. It must be small enough so that all of the sodium formed by dissociation is detected before reacting with the remaining Cl_2 . To detect at least 98% of this sodium, and with Cl_2 concentrations on the order of $0.4\text{--}1.0 \times 10^{13} \text{ cm}^3$ (large enough to react with Na in a distance much shorter than the distance from the oven to the photolysis region) the laser delay should be less than $3.0 \mu\text{s}$. On this time scale, the recoiling of photodissociated sodium will be thermalized. We measured the decrease in $[\text{Na}]_p$ as a function of delay time and observe a decay ($\tau \sim 100 \mu\text{s}$) commensurate with this secondary reaction with Cl_2 and with diffusion out of the detection region. On the other hand, it is desirable to have some delay so as to avoid any electronic interference or UV induced effects associated with the excimer pulse. Thus delays between 200 ns and $2.0 \mu\text{s}$ were used.

The most significant correction to the data arises in accounting for the different diffusivities of Na and NaCl. As mentioned above, Na emanating from the oven travels ~ 17 cm before being detected. When quantitatively converted to NaCl (in 1–2 cm), the NaCl then travels ~ 15 cm before detection. In our initial analysis above we have assumed that $[\text{NaCl}] = [\text{Na}]_0$ in the photolysis region. However, this is only approximately correct. Although true at the end of the narrow reaction zone, these species' axial concentrations will decay at different rates due to diffusion to and sticking on the reactor walls. A correction must therefore be made for the differing diffusivities of Na and NaCl. This is done according to the methods outlined in Ref. 21, using a measured diffusion coefficient for atomic sodium of $0.48 \text{ cm}^2 \text{ s}^{-1}$ at 1 atm and 300 K, and an approximate value for NaCl of $0.40 \pm 0.05 \text{ cm}^2 \text{ s}^{-1}$ at 1 atm.²² The underestimation of $[\text{NaCl}]$ in the photolysis region results in a reduction in R by

TABLE I. Measured photodissociation cross sections for NaCl.

Wavelength (nm)	Excimer gas	Raman-shifted line ^a	Number of measurements	Average cross section ^b (cm ²)
189.7	KrF	<i>AS</i> ₃ (H ₂)	2	6.12 ± 1.44 (− 18)
193.4	ArF	...	4	5.56 ± 1.06 (− 18)
203.1	KrF	<i>AS</i> ₃ (D ₂)	1	1.48 ± 1.40 (− 18)
205.3	ArF	<i>S</i> ₁ (D ₂)	1	9.06 ± 1.48 (− 19)
205.9	KrF	<i>AS</i> ₂ (H ₂)	2	8.96 ± 0.60 (− 19)
210.3	ArF	<i>S</i> ₁ (H ₂)	2	7.36 ± 0.59 (− 19)
216.3	KrF	<i>AS</i> ₂ (D ₂)	1	1.51 ± 0.67 (− 18)
218.7	ArF	<i>S</i> ₂ (D ₂)	2	4.63 ± 1.76 (− 19)
225.2	KrF	<i>AS</i> ₁ (H ₂)	4	1.46 ± 0.08 (− 18)
230.4	ArF	<i>S</i> ₂ (H ₂)	3	5.12 ± 0.40 (− 18)
231.2	KrF	<i>AS</i> ₁ (D ₂)	2	9.47 ± 0.80 (− 18)
234.0	ArF	<i>S</i> ₃ (D ₂)	2	1.30 ± 0.30 (− 17)
237.6	KrF	<i>S</i> ₁ (H ₂) + <i>AS</i> ₂ (D ₂) ^c	2	6.38 ± 1.31 (− 18)
241.4	KrF	<i>AS</i> ₁ (H ₂) + <i>S</i> ₁ (D ₂) ^c	2	6.74 ± 0.72 (− 18)
248.4	KrF	...	7	1.29 ± 0.05 (− 18)
251.6	ArF	<i>S</i> ₄ (D ₂)	1	2.51 ± 1.19 (− 18)
254.8	ArF	<i>S</i> ₃ (H ₂)	3	4.24 ± 0.41 (− 18)
260.2	KrF	<i>AS</i> ₁ (H ₂) + <i>S</i> ₂ (D ₂) ^c	1	4.33 ± 0.50 (− 18)
268.3	KrF	<i>S</i> ₁ (D ₂)	4	1.74 ± 0.23 (− 18)
277.0	KrF	<i>S</i> ₁ (H ₂)	6	4.00 ± 0.47 (− 19)
285.0	ArF	<i>S</i> ₄ (H ₂)	2	0 ± 1.8 (− 19)
291.8	KrF	<i>S</i> ₂ (D ₂)	2	8 ± 1 (− 21)
313.0	KrF	<i>S</i> ₂ (H ₂)	2	0 ± 8 (− 21)
319.6	KrF	<i>S</i> ₃ (D ₂)	1	0 ± 9 (− 21)
359.8	KrF	<i>S</i> ₃ (H ₂)	1	2.7 ± 3.1 (− 21)

^a Designation of Stokes or anti-Stokes line with gas used in the Raman-shift cell in parentheses. Gas cell pressures were 125 psig for H₂ and 250 psig for D₂.

^b Exponent in parentheses; error is one standard deviation uncertainty in precision.

^c These are combination Raman-shift lines in a 25% H₂:75% D₂ mixture at 250 psig total pressure.

a factor of 1.4 ± 0.4 . This systematic error affects only the absolute magnitude of the photodissociation cross section curve as a function of wavelength, but not the relative shape of the curve.

RESULTS

Room temperature photodissociation cross sections for gaseous NaCl were measured at 25 wavelengths in the range 189.9–359.8 nm. A plot of the results is shown in Fig. 2. Error bars represent one standard deviation uncertainties in each point, excluding a systematic error of $\pm 30\%$ due to the correction for diffusion. This last uncertainty would have the effect of uniformly shifting the curve up or down. Table I lists the averaged data taken at each wavelength and illustrates the ability of this technique to accurately measure very small cross sections. Our results exhibit two distinct peaks and a rise in σ toward the shortest wavelengths. We do not observe any dissociation at energies below ~ 100 kcal mol^{−1} (285 nm), which is consistent with the currently accepted value for the bond strength of 98 ± 2 kcal mol^{−1}.^{9,23}

As seen in Fig. 2, the error bars for most points are less than 20%, except (unfortunately) at the center of the large peak at 234 nm. This point and the next two higher wavelength points were taken using very weak Raman-shifted lines (the latter two being combinations of Stokes and anti-Stokes lines),²⁴ so that there is a greater uncertainty in the absolute height of this peak as compared with the longer wavelength peak. For most points, the source of the error

bars lies in the absolute UV power measurement and not in the determination of the ratio of $[\text{Na}]_p/[\text{Na}]_0$.

DISCUSSION

The results presented in this work are in qualitative agreement with the earlier work of Davidovits and Brodhead.⁴ However, there are two significant differences: the resolution of the absorption peaks and the absolute magnitude of the cross sections. Gaseous alkali halides in the earlier work were produced in a heated reservoir and effused into a slightly warmer quartz absorption cell. For NaCl, cell temperatures were in the range of 1123–1223 K. At these temperatures, the first five vibrational levels account for over 90% of the population. One might expect broad absorption features since each excited vibrational state will dissociate over a different range of energies than for the ground vibrational state. In this work, NaCl is equilibrated with the flow carrier gas at 300 K, primarily populating only the ground and first excited vibrational states (83% and 14%, respectively), so that narrower peaks are not surprising.

The absolute magnitudes of the integrated cross sections for the data above 220 nm (see following discussion) calculated from the two sets of data pose a greater problem in that they differ by a factor of 6. The quoted error bars on both experiments do not account for this discrepancy and one suspects that either or both experiments contain systematic errors. One possible explanation is the presence of NaCl dimers in the high temperature experiments. Davidovits and Brodhead determined their absorption cross sections assum-

ing that NaCl monomer, calculated from tabulated vapor pressure curves, was the sole absorber in their cell. They also estimated the fraction of $(\text{NaCl})_2$ in their experiments to be 40%–60%. If these absorbed light to form either $\text{Na} + \text{NaCl}_2$ or 2NaCl , the overall number density of absorbers would be larger and the reported cross section values lower.

No dimers are present in our experiments. Sodium chloride is formed by chemical reaction in a flowing carrier gas and there are insufficient collisions for dimerization to occur via termolecular recombination. Lamb and Benson²⁵ have calculated the rate constant for



to be $k = 10^{-28.5} \text{ cm}^6 \text{ molecule}^{-2}$ at 230 K. Assuming this value to be approximately the same at 300 K, less than 0.002 of the nascent NaCl dimerizes over the path between where it is formed and the photolysis volume.

Absorption in the ultraviolet has been observed for dimeric species such as $(\text{NO})_2$ and $(\text{N}_2\text{O})_2$.^{26–28} These absorptions occur in the same spectral region as absorptions of the monomer and, at least in the case for $(\text{NO})_2$, exhibits a large oscillator strength.²⁶ This suggests that it is possible for even a weakly bound dimer to exhibit a strong UV absorption cross section. On the other hand, Su and Riley did not observe any anomalous features in their time-of-flight recoil distributions of alkali halides, photodissociated at 266 nm, which suggest the presence of dimers.^{7–9} Oppenheimer and

Berry did not observe any features attributable to dimers for matrix isolation measurements of LiI, NaBr, and NaI, where dimers would be expected to be present.²⁹ For NaCl, KI, RbBr, and LiBr, no absorption bands attributable to any species were observed.

The only other comparable alkali halide cross section measurement at room temperature is that for CsI by Grossman *et al.*⁶ The results are consistent with our measurements for NaCl. The spectral width for this $1\text{-}^1\Sigma^+$ transition [in Hund's case (c) notation] is narrower and the integrated cross section is a factor of 2 smaller than that reported by Davidovits and Brodhead.⁴ Furthermore, cesium iodide dimers are not expected to be present in either experiment.

Cross section calculations

The ionic ground electronic state for the lighter alkali halides is designated $X^1\Sigma^+$ [Hund's case (a)], and correlates to separated $\text{M}^+ + \text{X}^-$ ions. Excited molecular states correlating with neutral atoms $\text{M} + \text{X}$ are covalent, and for $\text{Na}(^2S) + \text{Cl}(^2P_J)$, are represented by Hund's case (c) angular momentum coupling as $\Omega = 0^+, 0^-, 1$, and 2 .^{1,30} Only $0^+ \leftarrow 1^1\Sigma^+$ (parallel) and $1 \leftarrow 1^1\Sigma^+$ (perpendicular) transitions are allowed. The potential curve for the ground electronic state of these molecules is fairly well represented by a modified Rittner potential, reproducing experimentally measured dissociation energies and anharmonic constants with reasonable accuracy (see Fig. 3).³¹

The first few electronic excited state potentials are not well characterized. They are thought to be either repulsive or only slightly bound.^{1,4} Zeiri and Balint-Kurti¹⁴ have calculated the ground and first four excited electronic state potentials and associated transition dipole moments for a group of alkali halides using a semiempirical valence-bond method, while excluding the effects of spin-orbit coupling. Within the framework of this Hund's case (a) approach, they find that the excited states are all fairly repulsive (see Fig. 3) and that use of the Franck-Condon approximation is invalid here as the transition dipole moments vary considerably with internuclear separation r . Their excited state curves are labeled in $1^1\Sigma^+$ (parallel) and $1^1\Pi$ (perpendicular) notation.

In order to gain a clearer understanding of our results, we have calculated NaCl absorption cross section curves over the wavelength range 180–300 nm for comparison with our experimental data. We use the reflection approximation³² in which the electronic transition moment is calculated using a harmonic oscillator wave function for the ground electronic state, a δ function for the upper repulsive state wave function, and Zeiri's transition dipole moments at each value of r . At 300 K, only $v = 0$ and $v = 1$ are sampled, so that the harmonic oscillator potential accurately represents the Rittner form (see insert in Fig. 3). Small corrections for the displacement of higher vibrational levels from the equilibrium internuclear separation r_e , and for the effect of thermally averaged rotational populations on the absorption wavelengths were also included in this calculation.

Figure 4 compares the calculated and experimental data. In all cases, the total integrated cross section for the sum of the $A\text{-}X$ and $B\text{-}X$ transitions for calculated curves have been normalized to that of the experimental curves.

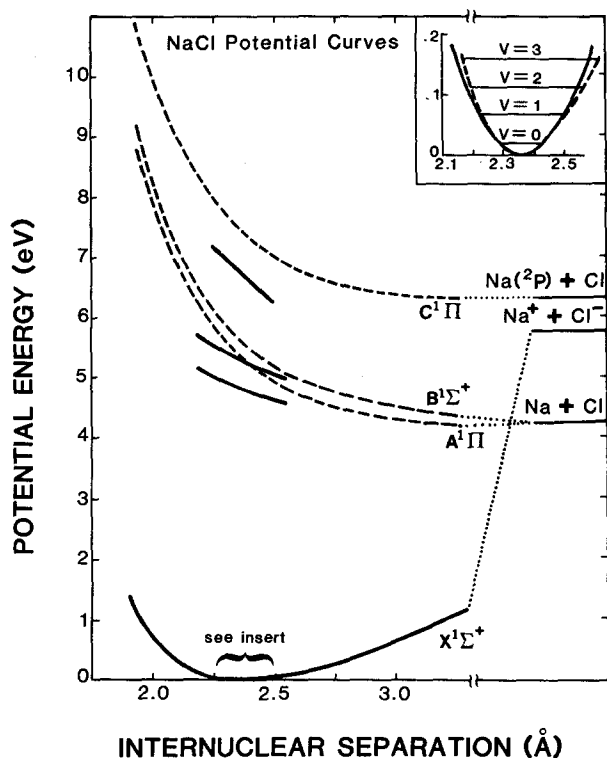


FIG. 3. Potential curves used in the calculation of NaCl photodissociation cross sections. Dashed lines are the calculated curves of Zeiri and Balint-Kurti (Ref. 14). Solid lines (for $A^1\Pi$, $B^1\Sigma^+$, and $C^1\Pi$) are derived as discussed in the text. The insert shows the lowest part of the $X^1\Sigma^+$ potential, and illustrates how the harmonic oscillator approximation (solid curve) compares with the Rittner potential (dashed curve) (Ref. 31) for the lower vibrational levels.

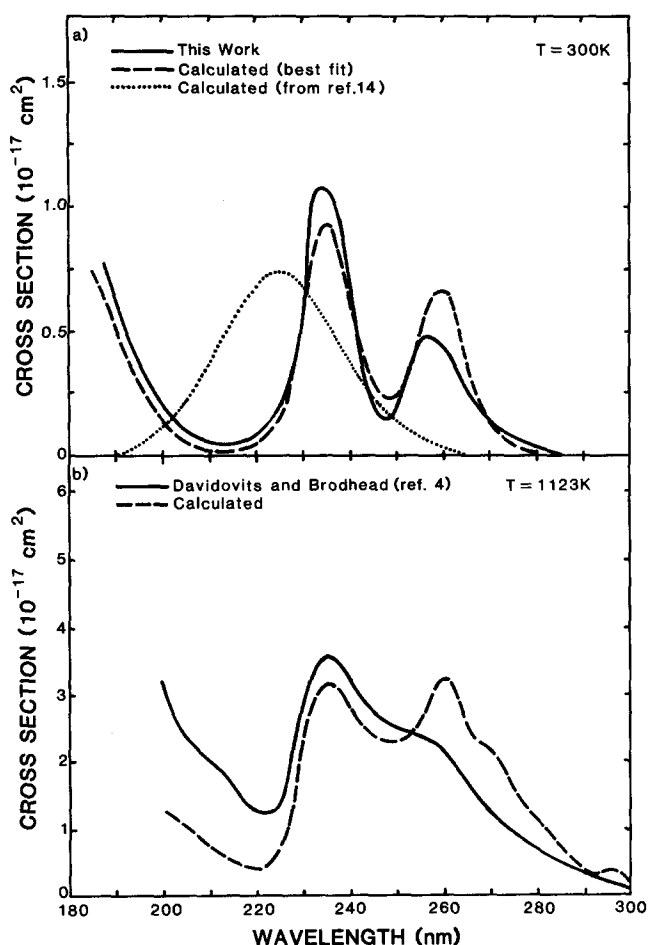


FIG. 4. Plots of experimental data vs calculated cross section curves. (a) 300 K data using representative experimental curve from Fig. 1. (b) 1123 K data of Davidovits and Brodhead (Ref. 4). The computed curves have been normalized to have equal total integrated cross sections above 220 nm (sum of the $A-X$ and $B-X$ transitions).

The dotted curve in Fig. 4(a) shows the absorption curve at 300 K calculated from the potentials of Zeiri and Balint-Kurti.¹⁴ This curve, which does not match the experimental data (represented by the solid curve), is shifted to much shorter wavelengths and exhibits one broad peak. Transitions to both the $A^1\Pi$ and $B^1\Sigma^+$ states lie under this peak. Excitations to higher states lie further into the ultraviolet.

To better reproduce our experimental results, we varied the energies and shapes of the $A^1\Pi$, $B^1\Sigma^+$, $C^1\Pi$, and $D^1\Sigma$ states in a narrow region of $\pm 0.25 \text{ \AA}$ about $r_e = 2.36 \text{ \AA}$. This range corresponds to the values of r over which the square of the lowest five vibrational wave functions are important. For $v=0$ and $v=1$, only the region $\pm 0.10 \text{ \AA}$ about R_e contributes to σ , and the best fit to our data only senses this range of r . The results of this fit to our data are shown as the dashed curve in Fig. 4(a) and results from lowering all four curves and flattening the A and B states in the region about r_e (Fig. 3). These new curves are reasonable in light of the approximations made by Zeiri and Balint-Kurti.¹⁴ They state that no valence-bond structures corresponding to Rydberg states were included in their

calculations, and the inclusion of these states would have made their calculated repulsive curves less repulsive.

The peaks at 235 and 260 nm in Fig. 4(a) represent the $B-X$ (parallel) and $A-X$ (perpendicular) transitions, respectively. At wavelengths shorter than 220 nm, the $C-X$ (and $D-X$) transition causes the cross section to rise, as observed in the data. We do not observe the peak absorption for this transition, so the shape and position of the $C^1\Pi$ data is less well determined than the A or B states. Nevertheless, the fact that this rise is seen at all near 200 nm strongly suggests that the $C^1\Pi$ state is bound, lying at energies which are equal to or slightly lower than the energy of its dissociation products, $\text{Na}(^2P) + \text{Cl}(^2P_j)$. This has been observed for this state in other alkali halides.²

The relative heights of the calculated peaks at room temperature agree qualitatively with the experimental data (normalized to total integrated cross section), suggesting that Zeiri's transition dipole moment calculations are approximately correct. Su and Riley measured the ratio of the parallel to total transitions moments at 266 nm for a series of alkali halides using a molecular beam recoil velocity technique.⁷⁻⁹ They find that the amount of parallel character drops from about 60% for the iodides to less than 30% for alkali chlorides. This ratio for NaCl was determined to be 0.16 ± 0.02 .⁹ At the temperature of their source (1189 K), we calculate a ratio of 0.28.

Using the potentials which were fit to our room temperature data, we computed the absorption spectrum at 1123 K for comparison with the experiments of Davidovits and Brodhead.⁴ Despite the limitations of the calculation (and uncertainties in extending them to high temperatures), we see in Fig. 4(b) that the agreement is remarkably good. The higher degree of structure in our calculations than were observed by Davidovits can be explained as arising from regions of r outside of $r_e \pm 0.10 \text{ \AA}$, so that small changes in the shapes of the potentials there would shift the absorption wavelengths and peak shapes for the excited vibrational states. Slightly steeper curves for $r < 2.2 \text{ \AA}$ would tend to broaden the absorption peaks for the higher vibrational states and lead to a smoother overall absorption curve.

In comparing the calculated ratio of the parallel to perpendicular transition probabilities to those observed by Davidovits and Brodhead,⁴ Su and Riley,⁹ and ourselves, this ratio is systematically high. This suggests that $B-X$ dipole transition moments of Zeiri and Balint-Kurti¹⁴ are too large relative to those of the $A-X$ transition.

In conclusion, photodissociation cross section measurements of NaCl at 300 K have resolved the $A-X$ and $B-X$ electronic transitions. From these spectra, more accurate potential curves for the $A^1\Pi$ and $B^1\Sigma^+$ electronic states have been derived in the region about the equilibrium internuclear distance of the NaCl ground state. The shape of the photodissociation spectrum is consistent with the photoabsorption spectrum of Davidovits and Brodhead,⁴ measured at 1123 K. However, the absolute magnitude of the integrated cross section in this work is about six times smaller than that of Davidovits. The most likely explanation is that the presence of dimers in the high temperature studies contributed to the observed absorption.

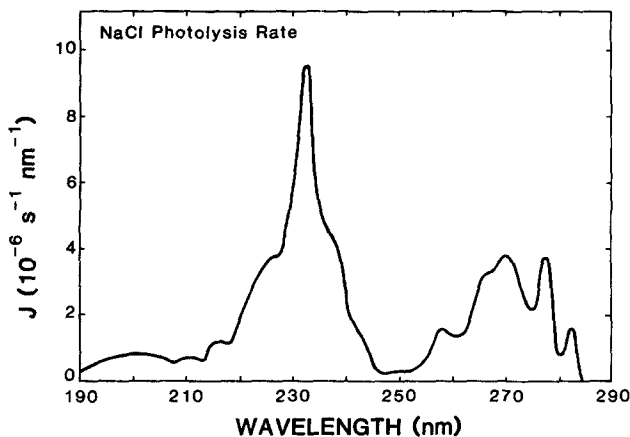


FIG. 5. Plot of the calculated photolysis rate of NaCl as a function of wavelength at 40 km altitude.

Stratospheric photolysis of NaCl

The photolysis of NaCl is crucial in determining the extent to which alkali metals of meteoric origin affect the ozone balance in the upper stratosphere.¹⁵⁻¹⁷ Convoluting the measured total solar flux at 40 km (including albedo and scattering)³³ over our measured cross sections between 180 and 300 nm, we obtain a total photolysis rate J of $1.9 \pm 0.8 \times 10^{-4} \text{ s}^{-1}$. Based on our calculations for cross sections, the curve at stratospheric temperatures ($\sim 260 \text{ K}$) is nearly the same as our 300 K results. This number is a factor of 10 smaller than that estimated by Rowland and Rogers¹⁷ using the high temperature data of Davidovits and Brodhead.⁴ The difference is due to two factors. First, the solar flux has a local minimum near 250 nm and falls off rapidly below 200 nm, offsetting much of the contribution of our peaks near 190, and 235 nm (Fig. 5). Second, the rapid rise in the solar flux above 270 nm overemphasizes excited vibrational state contributions to the cross section, which are absent at 40 km altitude (260 K).

Using $J = 1.9 \times 10^{-4} \text{ s}^{-1}$ and the measured rate constants for reactions (1)–(3),¹⁸⁻²⁰ the rate at which free chlorine is released from HCl at 40 km is $\sim 10^{-6} \text{ s}^{-1}$, where the photolysis of NaCl is the rate limiting step. This calculation assumes a total gas phase alkali concentration of $5 \times 10^5 \text{ cm}^{-3}$.³⁴ For comparison, the release rate of Cl for HCl by OH (i.e., $k_5 \cdot [\text{OH}]$) is $6.7 \times 10^{-6} \text{ s}^{-1}$, based on an OH concentration of 10^7 cm^{-3} and the value $k_5(260 \text{ K}) = 6.7 \times 10^{-13} \text{ cm}^3 \text{ s}^{-1}$.³⁵ Thus we conclude that, depending on the altitude at which heterogeneous and homogeneous removal processes of atmospheric alkali compounds dominate gas phase chemistry meteoric alkali chemistry could be an additional and important source of free chlorine in the upper stratosphere. We are presently investigating the magnitudes of processes through which atmospheric alkali compounds might be removed from the gas phase.

ACKNOWLEDGMENTS

The authors gratefully acknowledge helpful discussions with the late Professor Frederick Kaufman and the technical assistance of Warren E. Goodwin. This work was sponsored by the Fluorocarbon Program Panel of the Chemical Manufacturers Association under Contract No. FC-84-494 and by the Air Force Geophysics Laboratory under Contract No. F19628-83-C-0010.

- ¹R. S. Berry, in *Alkali Halide Vapors: Structure, Spectra and Reaction Dynamics*, edited by P. Davidovits and D. L. McFadden (Academic, New York, 1979), Chap. 3, and references therein.
- ²N. Furuta, E. Yoshimura, H. Haraguchi, and K. Fuwa, *Spectrochim. Acta Part B* **33**, 715 (1978), and references therein.
- ³D. F. Dever, B. Cardelino, and J. L. Gole, *High Temp. Sci.* **18**, 159 (1984).
- ⁴P. Davidovits and D. C. Brodhead, *J. Chem. Phys.* **46**, 2968 (1967).
- ⁵A. Mandl, in *Alkali Halide Vapors: Structure, Spectra, and Reaction Dynamics*, edited by P. Davidovits and D. L. McFadden (Academic, New York, 1979), Chap. 2.
- ⁶L. W. Grossman, G. S. Hurst, M. G. Payne, and S. L. Allman, *Chem. Phys. Lett.* **50**, 79 (1977).
- ⁷T.-M. R. Su and S. J. Riley, *J. Chem. Phys.* **71**, 3194 (1979).
- ⁸T.-M. R. Su and S. J. Riley, *J. Chem. Phys.* **72**, 1614 (1980).
- ⁹T.-M. R. Su and S. J. Riley, *J. Chem. Phys.* **72**, 6632 (1980).
- ¹⁰N. J. A. Van Veen, M. S. DeVries, J. D. Sokol, T. Baller, and A. E. DeVries, *Chem. Phys.* **56**, 81 (1981).
- ¹¹W. R. Anderson, B. M. Wilson, R. C. Ormerod, and T. L. Rose, *J. Chem. Phys.* **74**, 3295 (1981).
- ¹²P. Brumer and M. Karplus, *J. Chem. Phys.* **58**, 3903 (1973).
- ¹³R. N. Zare and D. R. Herschbach, *J. Mol. Spectrosc.* **15**, 462 (1965).
- ¹⁴Y. Zeiri and G. G. Balint-Kurti, *J. Mol. Spectrosc.* **99**, 1 (1983).
- ¹⁵E. Murad and W. Swider, *Geophys. Res. Lett.* **5**, 1035 (1978).
- ¹⁶E. Murad, W. Swider, and S. Benson, *Nature (London)* **289**, 273 (1981).
- ¹⁷F. S. Rowland and P. J. Rogers, *Proc. Natl. Acad. Sci. U.S.A.* **79**, 2737 (1982).
- ¹⁸J. A. Silver, M. S. Zahniser, A. C. Stanton, and C. E. Kolb, Twentieth Symposium (International) on Combustion, The Combustion Institute, 1984, p. 605.
- ¹⁹J. A. Silver and C. E. Kolb, *J. Phys. Chem.* (in press).
- ²⁰J. A. Silver, *J. Chem. Phys.* **84**, xxx (1986).
- ²¹J. A. Silver, A. C. Stanton, M. S. Zahniser, and C. E. Kolb, *J. Phys. Chem.* **88**, 3123 (1984).
- ²²J. A. Silver, *J. Chem. Phys.* **81**, 5125 (1984).
- ²³B. deB. Darwent, *Bond Dissociation Energies in Simple Molecules*, Natl. Stand. Ref. Data Ser., Natl. Bur. Stand No. 31 (U.S. GPO, Washington, D. C., 1970).
- ²⁴T. R. Loree, R. C. Sze, D. L. Barker, and P. B. Scott, *IEEE J. Quantum Electron.* **QE-15**, 337 (1979).
- ²⁵J. J. Lamb and S. W. Benson, *J. Geophys. Res.* (in press).
- ²⁶J. Billingsley and A. B. Callear, *Trans. Faraday Soc.* **67**, 589 (1971).
- ²⁷O. Kajimoto, K. Honma, and T. Kobayashi, *J. Phys. Chem.* **89**, 2725 (1985).
- ²⁸K. Honma and O. Kajimoto, *Chem. Phys. Lett.* **117**, 123 (1985).
- ²⁹M. Oppenheimer and R. S. Berry, *J. Chem. Phys.* **54**, 5058 (1971).
- ³⁰G. Herzberg, *Spectra of Diatomic Molecules* (Van Nostrand, New York, 1950), pp. 387-394.
- ³¹J. E. Szymanski and J. A. D. Matthew, *Can. J. Phys.* **62**, 584 (1984).
- ³²J. G. Winans and E. C. G. Stueckelberg, *Proc. Natl. Acad. Sci. U.S.A.* **14**, 867 (1928).
- ³³J. R. Herman and J. E. Mentall, *J. Geophys. Res.* **87**, 1319 (1982).
- ³⁴S. C. Liu and G. C. Reid, *Geophys. Res. Lett.* **6**, 283 (1979).
- ³⁵W. B. DeMore, J. J. Margitan, M. J. Molina, R. T. Watson, D. M. Golden, R. F. Hampson, M. J. Kurylo, C. J. Howard, and A. R. Ravishankara, NASA Jet Propulsion Laboratory Publication No. 85-37, 1985.